Generation of Solar Coronal White-light Images from SDO/AIA EUV Images by Deep Learning

Bendict Lawrance[1] ![ORCID], Harim Lee[1] ![ORCID], Eunsu Park[2] ![ORCID], Il-Hyun Cho[1] ![ORCID], Yong-Jae Moon[1,3] ![ORCID], Jin-Yi Lee[1] ![ORCID], Shanmugaraju A[4] ![ORCID], and Sumiaya Rahman[2]

[1] Department of Astronomy and Space Science, College of Applied Science, Kyung Hee University, Yongin, 17104, Republic Of Korea; moonyj@khu.ac.kr
[2] Space Science Division, Korea Astronomy and Space Science Institute, Daejeon, 34055, Republic of Korea
[3] School of Space Research, Kyung Hee University, Yongin, 17104, Republic Of Korea
[4] Department of Physics, Arul Anandar College, Karumathur 625514, Madurai District, Tamilnadu, India

Abstract

Low coronal white-light observations are very important to understand low coronal features of the Sun, but they are rarely made. We generate Mauna Loa Solar Observatory (MLSO) K-coronagraph like white-light images from the Solar Dynamics Observatory/Atmospheric Imaging Assembly (SDO/AIA) EUV images using a deep learning model based on conditional generative adversarial networks. In this study, we used pairs of SDO/AIA EUV (171, 193, and 211 Å) images and their corresponding MLSO K-coronagraph images between 1.11 and 1.25 solar radii from 2014 to 2019 (January to September) to train the model. For this we made seven (three using single channels and four using multiple channels) deep learning models for image translation. We evaluate the models by comparing the pairs of target white-light images and those of corresponding artificial intelligence (AI)–generated ones in October and November. Our results from the study are summarized as follows. First, the multiple channel AIA 193 and 211 Å model is the best among the seven models in view of the correlation coefficient (CC = 0.938). Second, the major low coronal features like helmet streamers, pseudostreamers, and polar coronal holes are well identified in the AI-generated ones by this model. The positions and sizes of the polar coronal holes of the AI-generated images are very consistent with those of the target ones. Third, from AI-generated images we successfully identified a few interesting solar eruptions such as major coronal mass ejections and jets. We hope that our model provides us with complementary data to study the low coronal features in white light, especially for nonobservable cases (during nighttime, poor atmospheric conditions, and instrumental maintenance).

Unified Astronomy Thesaurus concepts: Solar corona (1483); Astronomy data analysis (1858); Convolutional neural networks (1938); Solar atmosphere (1477); Solar extreme ultraviolet emission (1493); Solar coronal holes (1484); The Sun (1693)

Supporting material: animations

1. Introduction

Coronal white-light information helps us understand coronal features of the Sun, like helmet streamers (HSs), pseudostreamers (PSs), coronal mass ejections (CMEs), polar coronal holes, streamer waves, etc. (Gosling et al. 1976; Hundhausen et al. 1994; Yashiro et al. 2004; Schmit et al. 2009; Gopalswamy et al. 2013). In this regard, the white-light data from Mauna Loa Solar Observatory (MLSO), COronal Solar Magnetism Observatory (COSMO), and K-coronagraph (K-Cor) that observe the low corona in white light, which have the field of view (FOV) from 1.05 to 3 Rs, are considered valuable but rare. The K-Cor instrument at the ground-based MLSO (de Wijn et al. 2012) is dedicated to observing white-light low corona from 2013 to the present. This K-Cor was designed to study CMEs specifically and other coronal features in the white-light regime.

Ground-based observations such as the MLSO K-Cor have certain limitations: instrumental maintenance, poor atmospheric conditions, and nighttime nonavailability. While white-light coronagraph data in higher corona are available through the Solar and Heliospheric Observatory's (SOHO) Large Angle Spectrometric Coronagraph (LASCO; Brueckner et al. 1995), where C2's FOV is from 2 to 6 Rs and C3's FOV is up to 32 Rs, those in lower corona are very rare due to the nonavailability of C1 (FOV 1.1 to 3 Rs). In this sense, the MLSO K-coronagraph white-light data have been regarded to be very valuable as it observes low corona from 1.05 to 3 Rs.

Deep Learning is a branch of machine learning in artificial intelligence (AI) has been developed to learn the ways humans think based on artificial neural networks (Lecun et al. 1998, 2015). The convolutional neural network given by Lecun et al. (1998) is extensively used as a deep learning method regarding image translation. The deep learning model given by Goodfellow et al. (2014) based on Generative Adversarial Networks (GANs) distinguishes whether the generated image is real or fake by learning the loss. The conditional GANs (cGANs) developed by Isola et al. (2016) are considered to be very successful in resolving the image-to-image translation challenges. As mentioned above, considering the rareness of MLSO K-Cor images, we utilize the space-based Solar Dynamics Observatory/Atmospheric Imaging Assembly (SDO/AIA; Pesnell et al. 2012) images to generate the white-light images using a deep learning method to replace gaps in MLSO K-Cor data and to cover both the nonobservable time of this instrument and the nighttime from 1.11 to 1.25 Rs. This approach makes it possible to track the white-light coronal

features continuously. There are several deep learning methods reported and used to generate solar images and solar magnetograms (Park et al. 2018; Kim et al. 2019; Shin et al. 2020; Jeong et al. 2020; Lee et al. 2021). Recently, Son et al. (2021) generated ground-based He I 1083 nm images from SDO/AIA images through deep learning. In the present study, we utilize the deep learning method *pix2pi* to generate the ground-based MLSO K-Cor like white-light images from SDO/AIA images.

The generation of white-light coronal images by deep learning has several advantages. First, the ground-based MLSO K-Cor like white-light images from 1.11 to 1.25 Rs can be generated around the clock. Second, the generated white-light images will be helpful to fill data gaps and to track coronal features continuously during poor seeing atmospheric conditions and instrumental maintenance. Third, we can generate not only coronal holes and streamers, but also solar eruptions like jets and CMEs. The paper is organized as follows. The data and method are described in Section 2 and Section 3, respectively. The results and discussion are presented in Section 4 and the conclusion in Section 5.

2. Data

SDO/AIA is designed and dedicated in providing advanced high-quality EUV data with 12 s temporal resolution to study and understand the physics of the solar activities to the scientific community with an FOV up to 1.28 Rs. It is a space-based instrument where AIA is specifically designed to provide information in multiple wavelengths in view of the solar corona (Lemen et al. 2012). For this study, we collect three channels such as AIA 171, AIA 193, and AIA 211 Å as input data available from the Joint Science Operation Center (JSOC) database[5] to represent solar corona. We consider AIA 171, AIA 193, and AIA 211 Å for this study because the coronal features in the low coronal regions beyond the solar limb from 1 to 1.28 Rs are mostly clear and visible at these lines. In the case of other lines, the coronal features are less clear because they correspond to too hot temperatures (flaring) or low temperatures (chromospheric). MLSO COSMO K-Cor is a ground-based observatory operated by the High Altitude Observatory (HAO), a division of the National Center for Atmospheric Research (NCAR). It is dedicated to the study of the formation and the dynamics of low coronal features of the Sun in white light with an FOV from 1.05 to 3 Rs with a nominal cadence of 15 s. We collect MLSO K-Cor white-light data from the MLSO database.[6]

For training, validation, and evaluation data sets, we use SDO/AIA images and MLSO K-Cor white-light images. Though the FOV of MLSO K-Cor is from 1.05 to 3 Rs, the images are clear enough only from 1.11 Rs. Also, regarding SDO/AIA, though its FOV is up to 1.28 Rs, the images are clear only up to 1.25 Rs.

Considering these factors, we consider the FOV of the image pairs from 1.11 to 1.25 Rs for the study. Moreover, the MLSO K-Cor observatory can observe during the day (cadence 15 s), but SDO/AIA data is available around the clock with a time cadence of 12 s. Hence, considering these factors, we produced 21,071 pairs (from 1.11 to 1.25 Rs) of input and target images with a 20 minute cadence from 2013 October to 2019

December by careful visual inspection. We classify the data: January to September for training, October and November for testing, and December for validation.

We apply the data preprocessing to the white-light data and EUV data as follows. First, considering the FOV and the clarity of the images, we select the images from 1.11 to 1.25 Rs for our study. Second, white-light and EUV images are transposed into polar coordinates. Third, regarding the intensity, K-Cor white-light data are expressed in bolometric intensity (log scaled). To calibrate the EUV data, we divide them by the respective median intensity of the solar disk (B/BSun) to make the EUV data (log scaled) as reported in the K-Cor data. For image translation, we consider the solar coronal images in polar coordinates starting from the western equatorial region. The south western portion $(+60°)$ is added to the left side and the northwestern portion $(+60°)$ to the right side of each so that every transposed image can show coronal features near the western equatorial region properly.

3. Method

We utilize the pix2pix model by Isola et al. (2016) based on the GAN (Goodfellow et al. 2014). The pix2pix model that we considered in this study is a combination of the cGAN (Mirza & Osindero 2014) and the deep convolutional generative adversarial network (DCGAN; Radford et al. 2015). This pix2pix model is included with two networks called generator and discriminator. The generator will generate target-like images from the input images. Then, the generator will minimize the differences between the target images and the generated target-like images. Then, the discriminator part will distinguish the real image pairs from the generated image pairs. Here we consider cGAN as a loss function,

$$\mathcal{L}_{cGAN}(G, D) = \log D(I, T) + \log(1 - D(I, G(I))), \quad (1)$$

where G is the generator, D is the discriminator, I represents input data, and T represents the target data. Here, $G(I)$ represents an output from the generator for a given input image. While the generator tries to minimize the objective, the discriminator tries to maximize it.

The model proposed by Isola et al. (2016) considered 256×256 images for training. For this study we use all data as 1024 by 1024 so that we modify the data pipeline and the depth of the generator network (Figure 1). We consider seven deep learning models whose information is given in Table 1. We train the models with 1,500,000 iterations and save the generators for every 15,000 iterations. As a result, we got 100 generators (and the discriminators) for 1,500,000 iterations. Then, we select the best model by comparing the generated white-light images with target images, which gives the highest mean correlation coefficient (CC) value for the respective validation data set of the models considered.

4. Results and Discussion

Figure 2 shows the comparison among the target K-Cor white-light image made at 17:33:41 UT on 2019 November 11 and the corresponding AI-generated ones using the seven different models. We compare how well the coronal streamers (HS, PS, and coronal ray-like structures) and the polar coronal holes are generated as they are in the target images. It seems that PSs (possible PS reported in the HAO website), HSs (Abbo et al. 2015), coronal-ray-like structures in the polar regions
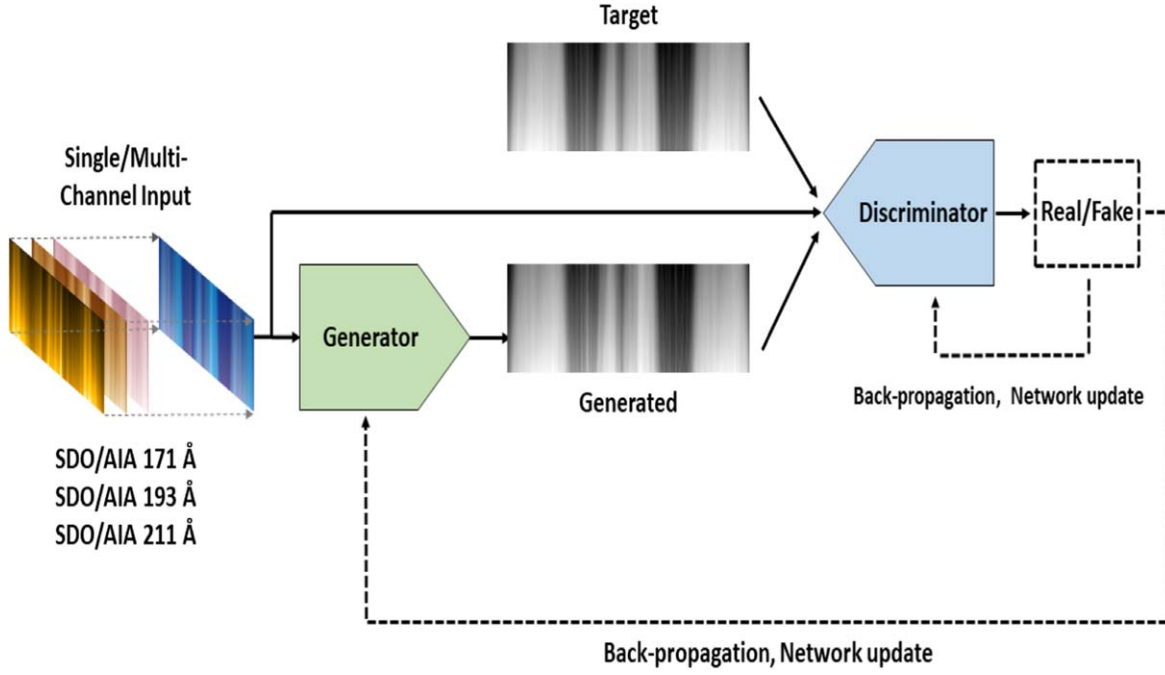

Target

Figure 1. Flowchart of our deep learning model (cGAN) used in this study.

Table 1
Comparison of Metrics for the Deep Learning Models Considered for the Validation Data Set in This Study

Metrics	Model 1	Model 2	Model 3	Model 4	Model 5	Model 6	Model 7
AIA Input (Å)	171	193	211	171+193	171+211	193+211	171+193+211
Normalized RMSE	0.098	0.087	0.085	0.084	0.083	0.080	0.076
Pearson's CC (pixel to pixel)	0.897	0.925	0.935	0.932	0.942	0.945	0.943

(Wang et al. 2007), and polar coronal holes are well generated by all of the models except for the first model. For example, the region between the PS and the HS (a region within the red box in Figure 2) on the eastern equator does not seem to be reproduced well by the first model (using AIA 171 Å). These coronal streamers and polar coronal holes seem to be well generated by all other models. Also, it should be noted that, the overall distribution of the target image seems well reproduced in the generated ones of all other models (Figure 2), but there are few differences between these models.

To test our results, we calculate the metrics like CC and normalized root mean square error (NRMSE). CC and NRMSE are calculated from each pair of generated and target white-light images. The results are shown in Table 1. The CC and NRMSE are given by

$$CC = \frac{\sum_{i=1}^{N}(X_i - \overline{X})(Y_i - \overline{Y})}{\sqrt{\sum_{i=1}^{N}(X_i - \overline{X})}\sqrt{\sum_{i=1}^{N}(Y_i - \overline{Y})}}, \qquad (2)$$

$$NRMSEi = \sum \frac{RMSE_i}{ymax - ymin}, \qquad (3)$$

where X represents the pixel values of the generated images, Y represents the pixel values of the real images, $\overline{X}$ represents the average pixel values of generated images, $\overline{Y}$ represents the average pixel values of real images, and N represents the total number of pixels, respectively. "RMSE" is the root mean

squared error. We estimate these metrics for a considered coronal region with 400×624 pixels.

We consider the best model, by comparing the highest mean CC value of the validation data set. Once the deep learning model is trained, the performance of the model will be measured using the validation data set. Based on the comparison, we find that the sixth model AIA 193 and 211 Å gives a CC value of 0.945 with a relatively small NRMSE, which is the best among the seven models. The test data set also confirms that Model 6 is the best with a CC value of 0.938. The results of the validation and the test data set are given in Tables 1 and 2. In addition to that, low coronal eruptions like CMEs/jets seem to be generated well by only Model 6 with AIA 193 and 211 Å. The ejection phenomena show up best in these AIA wavelengths. In this sense, we think that our selection is reasonable.

Next we compare polar coronal hole sizes to check how well our model generates the white-light images. We calculate the polar coronal hole sizes separately in the north and the south polar regions, based on the log-scaled intensity of the target and the AI-generated images. For example, the target K-Cor image observed at 19:38:52 UT on 2018 November 27 and the corresponding AI-generated image is shown in Figures 3(a) and (b).

In this study, we calculate the sizes of polar coronal holes as follows. First, we fix the mean log-scaled intensity separately for the north (horizontal green line) and the south polar regions (horizontal orange line) as shown in Figures 3(c) and (d). As
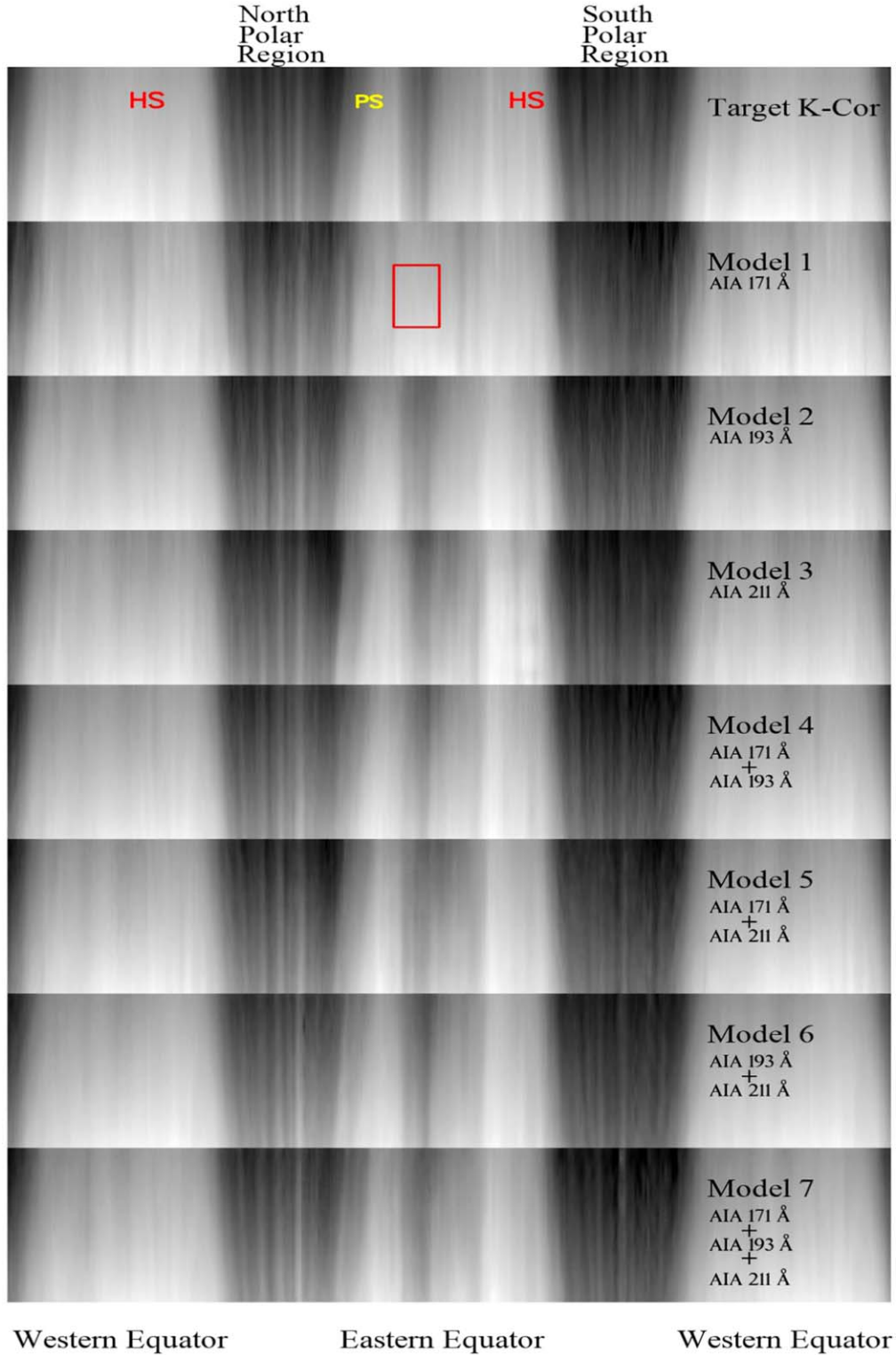
Figure 2. Comparison between the target K-Cor white-light image and the AI-generated images between 1.11 and 1.25 Rs based on single- and multichannel inputs at 17:33:41 UT on 2019 November 11. Note: the solar coronal images are considered in polar coordinates (Azimuth angle) starting from the westward equatorial region for this study. Helmet streamers (HSs) and pseudostreamer (PS). The red box represents the region not well identified by Model 1.

seen in the figure, the intensity is much lower in the polar coronal hole regions than in the equatorial regions. It is important to emphasize here that polar coronal hole regions are open magnetic field regions that are responsible for high-speed solar winds (Krieger et al. 1973). In this perspective, the northern and the southern polar coronal hole regions look dark in white light, due to low gas density in comparison with the bright structures such as HSs, which have enhanced gas density in the eastern and the western equators (Charbonneau & Hundhausen 1996). Second, we calculate the distance between

Table 2
Comparison of Metrics for the Deep Learning Models Considered for the Test Data Set in This Study

Metrics	Model 1	Model 2	Model 3	Model 4	Model 5	Model 6	Model 7
AIA Input (Å)	171	193	211	171+193	171+211	193+211	171+193+211
Normalized RMSE	0.116	0.106	0.109	0.101	0.098	0.089	0.094
Pearson's CC (pixel to pixel)	0.890	0.913	0.927	0.923	0.936	0.938	0.936
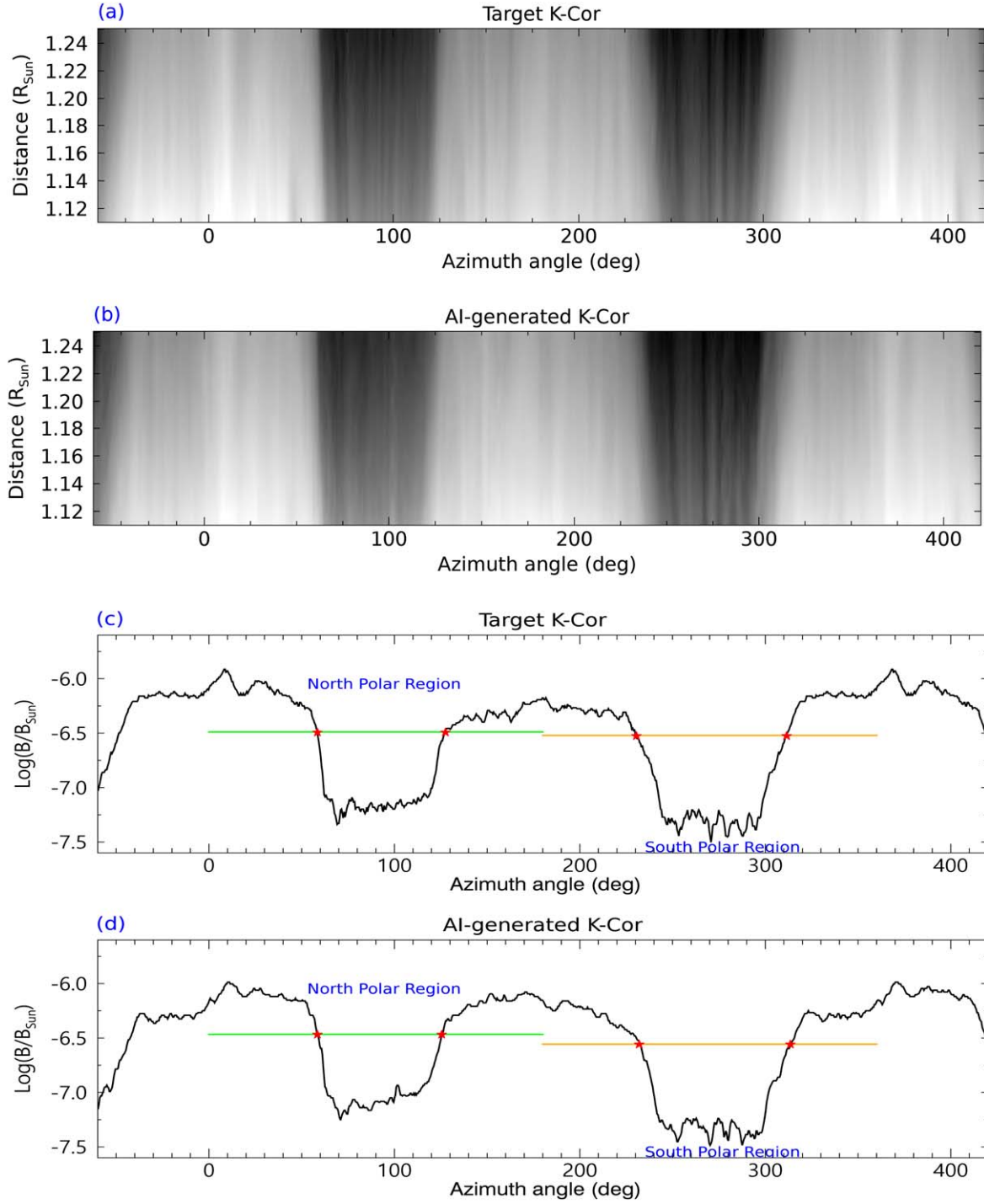
Figure 3. Comparison of polar coronal hole sizes of the (a) target K-Cor observation on 2018 November 27 at 19:38:52 UT, the (b) corresponding AI-generated image, and the intensity map of (c) target K-Cor and (d) AI-generated images.

Table 3
Comparison of Polar Coronal Hole Sizes of the Target and the AI-generated Images

| Date | Time (UT) | Polar Coronal Hole Size (deg) | | | |
| | | Target | | Generated | |
		North Pole	South Pole	North Pole	South Pole
2016/Oct/11	19:19:51	79	69	83	73
2016/Nov/02	17:40:18	91	59	91	63
2016/Nov/04	22:26:37	78	71	81	75
2016/Nov/05	21:15:19	76	72	79	75
2016/Nov/11	21:18:35	68	77	75	79
2017/Oct/01	17:20:32	72	75	68	75
2017/Oct/02	17:37:11	79	75	87	70
2017/Oct/27	17:47:52	69	81	68	81
2017/Oct/28	20:45:54	74	75	72	75
2017/Oct/29	18:46:10	75	71	77	70
2017/Nov/09	00:04:22	64	90	62	84
2017/Nov/24	21:14:01	70	76	73	69
2018/Oct/24	18:21:42	64	85	64	80
2018/Nov/29	17:33:41	78	70	78	65
2018/Nov/19	17:48:53	71	83	71	84
2018/Nov/21	18:44:06	73	75	73	79
2018/Nov/27	19:38:52	81	63	80	66
2018/Nov/20	19:44:33	69	83	71	78
2019/Oct/17	17:48:38	74	78	75	80
2019/Oct/27	22:44:21	73	80	75	76
2019/Nov/01	19:28:40	73	84	71	82
2019/Nov/02	17:32:17	72	85	69	86
2019/Nov/11	17:33:47	79	78	76	81
2019/Nov/11	19:33:47	78	83	71	82
2019/Nov/18	18:43:08	79	94	73	93

the junctures (marked by red star signs in the horizontal green line of the north polar region) considering from left to right (see Figures 3(c) and (d)).

We consider 25 AI-generated events by careful visual inspection of the test results (October and November). The images that have clear polar coronal holes with a relatively fewer number of plumes or coronal ray-like structures are considered to calculate the polar coronal hole sizes (Table 3) and to compare them with the target events. We found that, most of the polar coronal hole sizes were similar to each other. The average difference and the standard deviation between the polar coronal sizes of the target and the AI-generated ones are $-0.14°$ and $3.52°$, respectively. The distribution of polar coronal hole sizes of the target and the AI-generated ones are shown in Figure 4. It seems from the distribution that the polar coronal holes sizes of the AI-generated images using this deep learning model are consistent with the target images.

Next, we utilize our model to compare the generation of jet eruptions with the target ones. For this we consider the jet eruption observed by the MLSO K-cor instrument at 18:43:12 UT to 18:53:12 UT on 2016 March 10. The images from this jet eruption have not been included in the training part. We consider the importance of the jet eruption and choose this event for testing our model. It is very impressive that our model successfully generates this jet eruption (Figure 5(b)), which is consistent with the corresponding target images (Figure 5(a)).

This coronal jet started to erupt around 18:46:00 UT and ended around 18:53:00 UT in view of the MLSO K-Cor instrument. Similarly, we notice that the generated images of this jet eruption match with the same starting and ending times
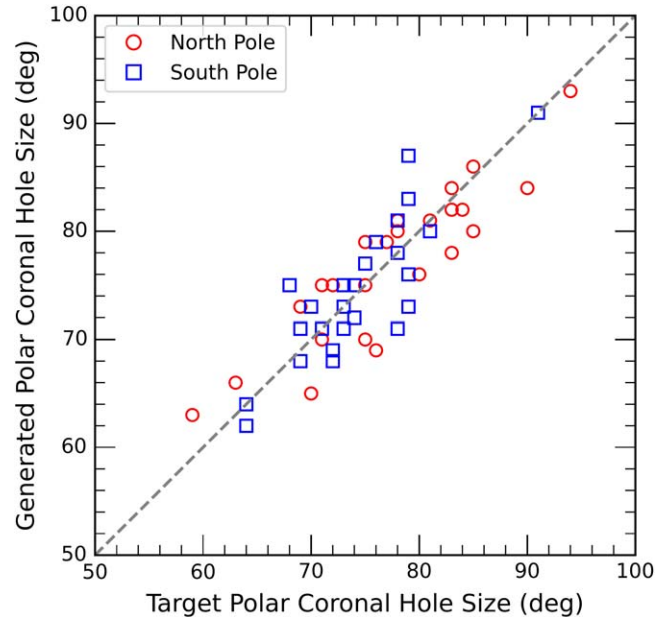

Figure 4. Distribution of the target and the AI-generated polar coronal hole sizes.

as observed by the MLSO K-Cor instrument. Hence, it seems that the jet eruption in a white-light regime could be made during nonobservable cases of the MLSO K-Cor from 1.11 to 1.25 Rs using the SDO/AIA images and using our model. Due to the occulting disks of the space-borne coronagraphs, the
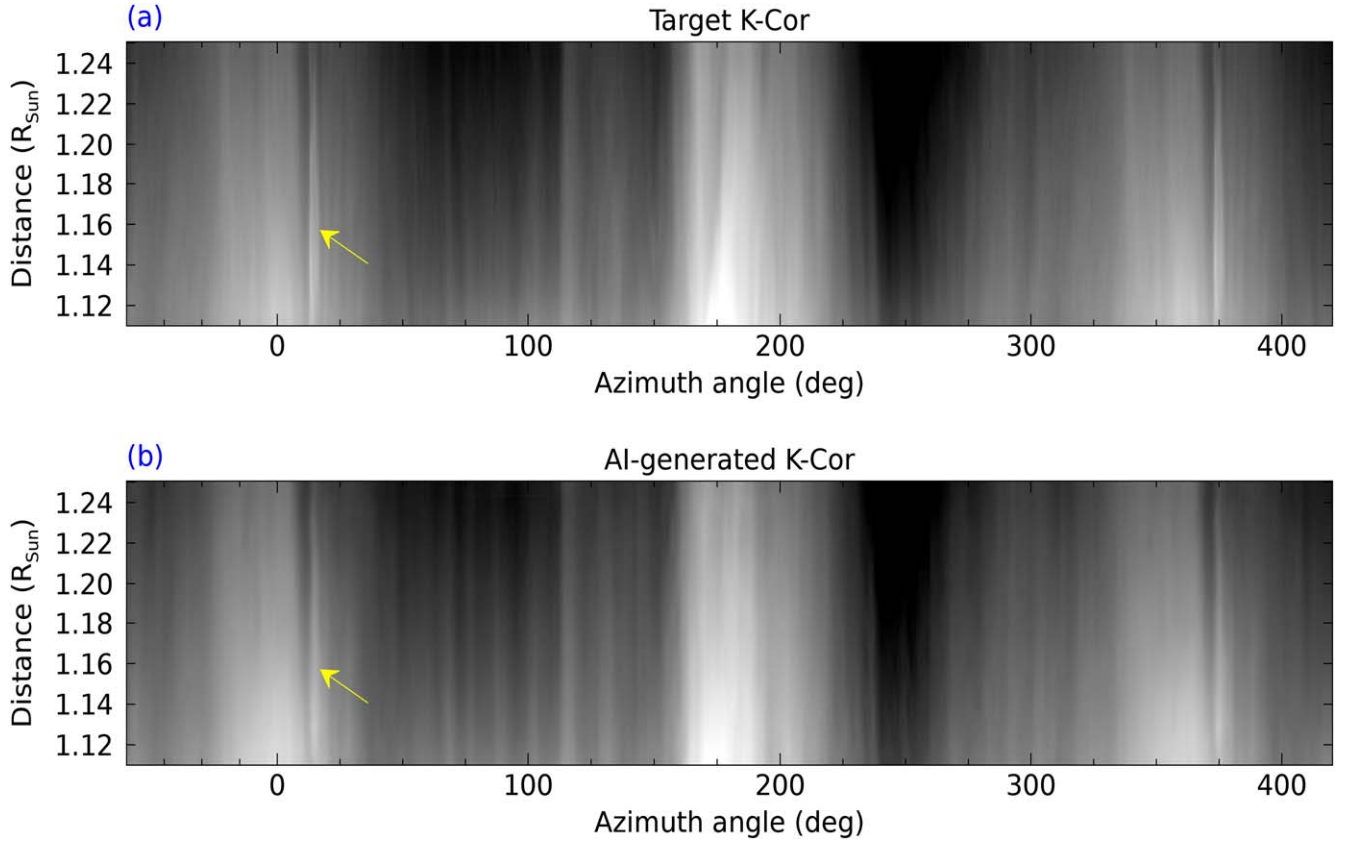
Figure 5. Coronal jet eruption at 18:49:10 UT on 2016 March 10. (a) Jet eruption (yellow arrow) observed by K-Cor instrument. (b) AI-generated image of this jet eruption. An animation of this figure with a 12 s cadence is available. The animation starts at 18:43:11 UT and ends at 18:53:11 UT where the jet eruption can be seen clearly.

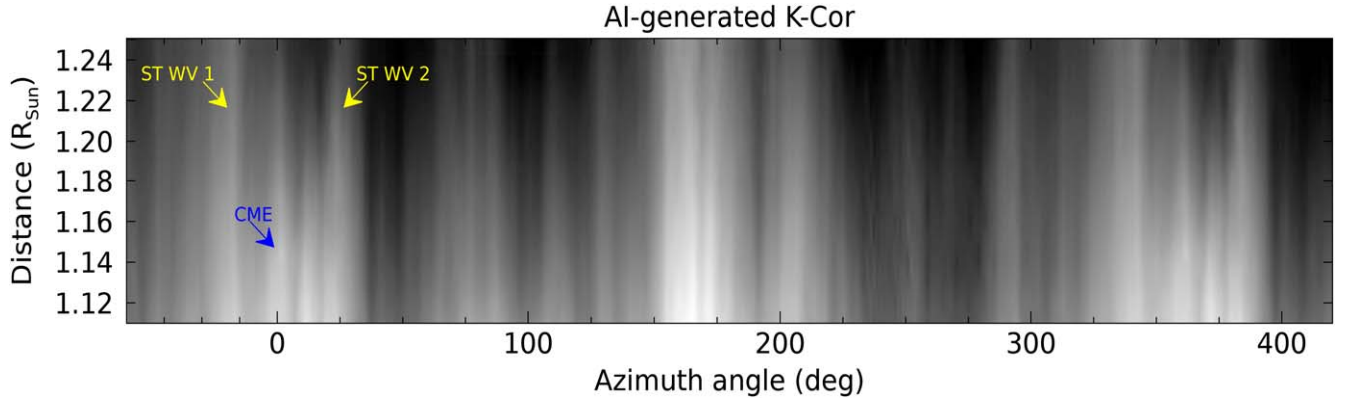(An animation of this figure is available.)

Figure 6. AI-generated CME–streamer wave interaction on 2012 May 17 (01:33:37 UT). Note: ST WV—streamer wave (indicated by yellow arrows) and CME—coronal mass ejection (indicated by a blue arrow). An animation of this figure is available. The animation starts at 01:19:37 UT and ends at 01:49:13 UT, in which the CME eruption, the interaction between the CME and streamer wave 1, and the recovery phase of the streamer wave after deflection are seen.

(An animation of this figure is available.)

solar corona is being observed beyond 2.0 Rs by LASCO C2. Thus it seems difficult to detect the less energetic jets (Hanaoka et al. 2018) by these white-light space-borne coronagraphs. Under those circumstances, scientists could rely on the EUV observations like SDO/AIA and Solar Ultraviolet Imager for the low coronal information on jet eruptions. Considering this issue, we hope that our model can be used to complement white-light data to study jet eruption in low corona from 1.11 to 1.25 Rs during the nonobservable cases.

The CME–streamer wave interactions in the low corona are well generated by our model. For example, we considered the 2012 May 17 CME event that seemed to interact with the coronal streamer wave (Rouillard et al. 2016; Decraemer et al. 2020) as seen clearly in the LASCO C2 and C3 coronagraphs around 02:00 UT. It is noted that these types of interactions can be seen through the EUV observations by SDO/AIA. In fact, the white-light images of this event in the K-Cor instrument are not available. The CME eruption (in white light) seems to be
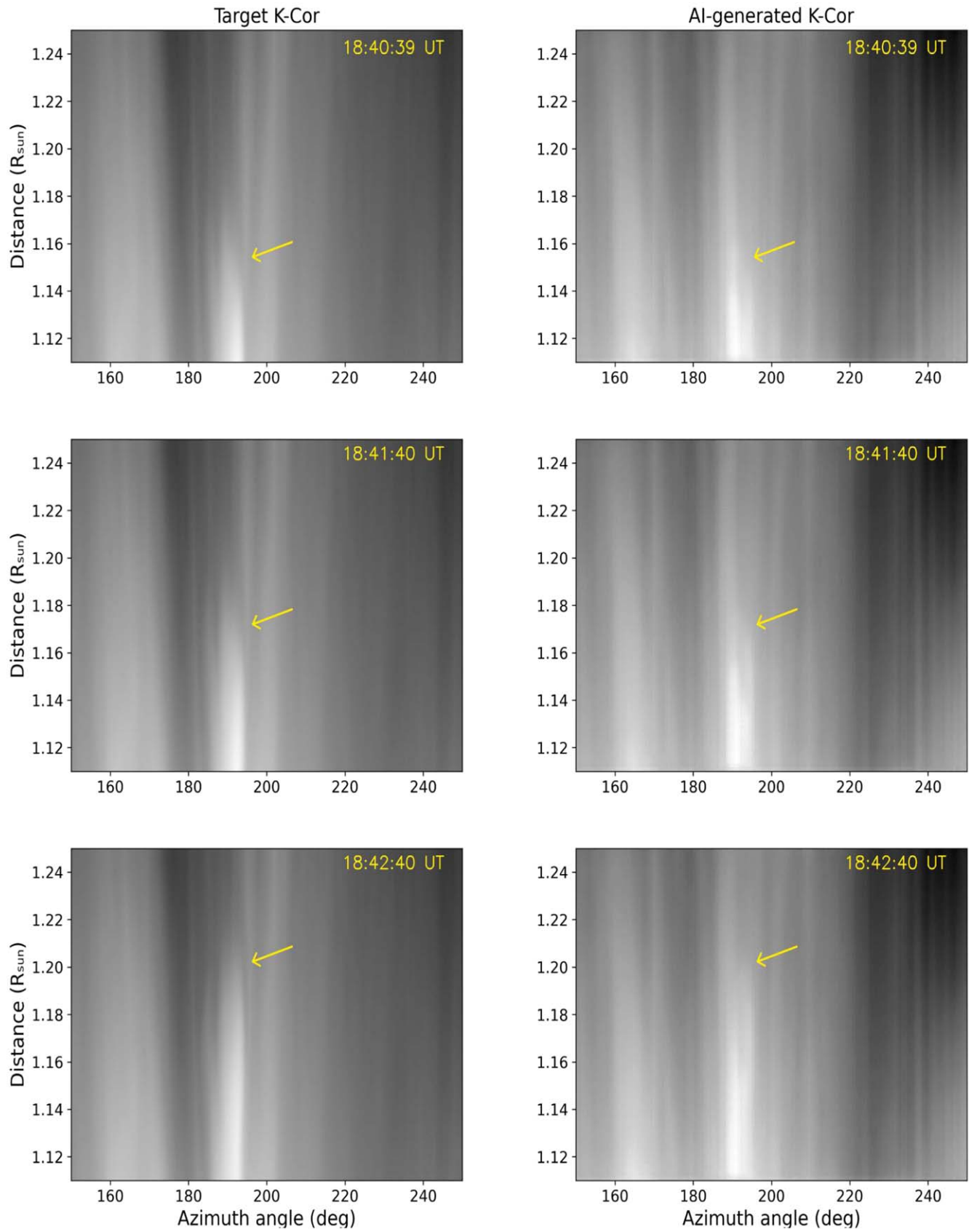
Figure 7. CME eruption on 2014 October 14. Left: CME eruption (yellow arrow) observed by K-Cor instrument. Right: AI-generated images of this CME eruption. An animation of this figure with a 12 s cadence is available.
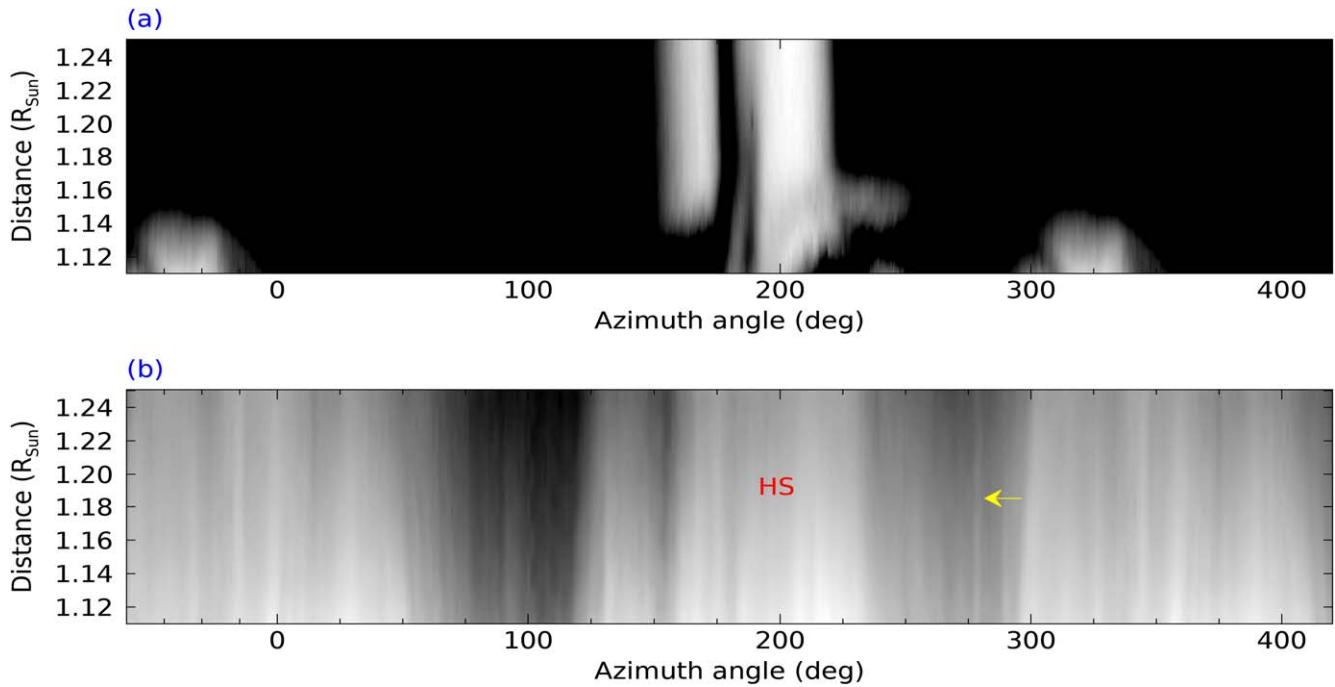
(An animation of this figure is available.)

Figure 8. (a) Poor quality image observed by K-Cor at 20:06:38 UT on 2017 February 2. (b) Replaced K-Cor-like AI-generated image by this model. Note: the yellow arrow in the south polar region indicates the coronal ray-like structure and HS indicated the helmet streamer.

well generated by using our model in comparison with the SDO/ AIA images. As additional data, the generated images would be useful in white-light counterparts as well. We notice the CME-flank and streamer wave (ST WV1) interaction between 01:33:37 to 01:36:15 UT within 1.25 Rs (see Figure 6). The interaction started around 01:34:38 UT and the full deflection can be seen at 01:37:13 UT. The recovery phase of the streamer wave started around 01:39:37 UT. It is noted that, these types of interactions can be seen through SOHO LASCO's C2 and C3 at greater heights. It is very impressive that our model could be useful to detect these types of interactions between 1.11 and 1.25 Rs in white light at an earlier time than SOHO LASCO's C2 and C3.

Next, we utilize our model to check how well our model generates the CMEs reported in the MLSO catalog. For this, we consider the test period used in this study of every year from 2013 to 2019 (October and November). As a result, we found 25 CMEs reported in the MLSO CME list. Out of these 25 CMEs, 5 CMEs are found to be major CMEs, 15 are faint CMEs, and the remaining 5 are very faint, in which the starting and ending times are difficult to conclude and not reported in the MLSO catalog. Then we utilize our model to check these remaining 20 CMEs. We found that the major CMEs seem to be generated well by our model. The faint CMEs are not well generated by our model, which is the limitation of this study. The major CMEs seem to be better well generated than the faint CMEs. For example, a major CME on 2014 October 14 event is shown in Figure 7. The starting and ending time of the AI-generated images of this CME eruption match with the target ones of the MLSO K-Cor.

Next, we utilize our model to generate the K-Cor white-light images during the observation time in poor visibility conditions of the MLSO K-Cor instrument. From the HAO website, we can see some reports related to poor quality data; they are classified as noisy, poor, and degraded. Hence, difficulties arise in confirming the coronal features, which lead to interruptions in continuous monitoring of them in white light. Considering

this issue, we generate white-light images to replace such kinds of images with poor quality by our model.

Our model is used to replace one such poor quality image of the K-Cor observation (Figure 8(a)) made at 20:06:38 UT on 2017 February 2 by the AI-generated one. It seems that the image is well generated (Figure 8(b)) by our model. For example, the HS (as shown in Figure 8(b)) in the eastern equator is restored well in the generated image. Also the coronal ray-like structure (indicated by a yellow arrow) seems to be restored well at the southern polar region. Hence, this model can be used to restore data during situations like poor visibility/degraded times to confirm coronal features, which makes it possible to have continuous monitoring of solar eruptions in white light, as well as to cover the data gap.

5. Conclusion and Summary

In this study, we have applied a deep learning method based on conditional generative adversarial networks to the generation of MLSO K-Cor-like white-light images from SDO/AIA images. We consider 21,071 pairs (between 1.11 and 1.25 Rs) of the MLSO K-Cor and the SDO/AIA (171, 193, and 211 Å) images from 2013 to 2019 for this study. We have made seven deep learning models (three using single channels and four using multiple channels). The major results of this study are summarized as follows. First, among the seven models considered, the multichannel model AIA 193 and 211 Å (Model 6) generates the coronal white-light images successfully with CC = 0.938. The AI-generated images of this model seem consistent with the target images. Second, the white-light images of dominant low coronal features such as HSs, PSs, polar coronal holes, and coronal ray-like structures are successfully generated. The positions and sizes of the polar coronal holes in the AI-generated images are consistent with those in the target ones. Third, using this model, it is impressive to note that we could generate major jet eruptions and CMEs.

The starting and ending times of the AI-generated images of the jet eruption considered in this study match with the target ones of the MLSO K-Cor. Our model could provide the data during the nonobservable cases of the MLSO K-Cor instrument and during the nighttime. This model will be useful to replace poor quality data such as noisy, degraded ones, data observed in poor atmospheric conditions, and during the instrumental maintenance of the MLSO K-Cor.

We would like to stress the advantage of this study is that the major CMEs/jets, polar coronal holes, HSs, and PSs in white light can be generated by our model once the SDO/AIA EUV images are available. In this regard, we hope that our model will be helpful in space weather forecasting of white-light counterparts. Next, by utilizing the AI-generated white-light images by our model, early coronal signatures like major CMEs/jets and other possible features can be detected in the low corona from 1.11 to 1.25 Rs at an earlier time than by SOHO LASCO's C2 and C3 telescopes. In this regard, we hope that our model will complement the nonavailability of the C1 telescope of the SOHO/LASCO satellite to a certain extent. In the future, we plan to generate SDO/AIA-like EUV images beyond its FOV utilizing the white-light images of the MLSO K-coronagraph.

ORCID iDs

Bendict Lawrance ⓘ https://orcid.org/0000-0001-6648-0500
Harim Lee ⓘ https://orcid.org/0000-0002-9300-8073
Eunsu Park ⓘ https://orcid.org/0000-0003-0969-286X
Il-Hyun Cho ⓘ https://orcid.org/0000-0001-7514-8171
Yong-Jae Moon ⓘ https://orcid.org/0000-0001-6216-6944
Jin-Yi Lee ⓘ https://orcid.org/0000-0001-6412-5556
Shanmugaraju A ⓘ https://orcid.org/0000-0002-2243-960X

References

Abbo, L., Lionello, R., Riley, P., et al. 2015, SoPh, 290, 2043
Brueckner, G. E., Howard, R. A., Koomen, M. J., et al. 1995, SoPh, 162, 357
Charbonneau, P., & Hundhausen, A. J. 1996, SoPh, 165, 237
de Wijn, A. G., Burkepile, J. T., Tomczyk, S., et al. 2012, Proc. SPIE, 8444, 84443N
Decraemer, B., Zhukov, A. N., & Van Doorsselaere, T. 2020, ApJ, 893, 78
Freeland, S. L., & Handy, B. N. 1998, SoPh, 182, 497
Goodfellow, I. J., Pouget-Abadie, J., Mirza, M., et al. 2014, arXiv:1406.2661
Gopalswamy, N., Xie, H., Akiyama, S., et al. 2013, ApJL, 765, L30
Gosling, J. T., Hildner, E., MacQueen, R. M., et al. 1976, SoPh, 48, 389
Hanaoka, Y., Hasuo, R., Hirose, T., et al. 2018, ApJ, 860, 142
Harris, C. R., Millman, K. J., van der Walt, S. J., et al. 2020, Natur, 585, 357
Hundhausen, A. J., Burkepile, J. T., St., & Cyr, O. C. 1994, JGR, 99, 6543
Isola, P., Zhu, J.-Y., Zhou, T., & Efros, A. A. 2016, arXiv:1611.07004
Jeong, H.-J., Moon, Y.-J., Park, E., et al. 2020, ApJL, 903, L25
Kim, T., Park, E., Lee, H., et al. 2019, NatAs, 3, 397
Krieger, A. S., Timothy, A. F., & Roelof, E. C. 1973, SoPh, 29, 505
Lecun, Y., Bengio, Y., & Hinton, G. 2015, Natur, 521, 436
Lecun, Y., Bottou, L., Bengio, Y., & Haffner, P. 1998, IEEEP, 86, 2278
Lee, H., Park, E., & Moon, Y.-J. 2021, ApJ, 907, 118
Lemen, J. R., Title, A. M., Akin, D. J., et al. 2012, SoPh, 275, 17
Mirza, M., & Osindero, S. 2014, arXiv:1411.1784
Mumford, S., Freij, N., Christe, S., et al. 2020, JOSS, 5, 1832
Park, E., Moon, Y.-J., Shin, S., et al. 2018, ApJ, 869, 91
Pesnell, W. D., Thompson, B. J., & Chamberlin, P. C. 2012, SoPh, 275, 3
Radford, A., Metz, L., & Chintala, S. 2015, arXiv:1511.06434
Rouillard, A. P., Plotnikov, I., Pinto, R. F., et al. 2016, ApJ, 833, 45
Schmit, D. J., Gibson, S., de Toma, G., et al. 2009, JGRA, 114, A06101
Shin, G., Moon, Y.-J., Park, E., et al. 2020, ApJL, 895, L16
Son, J., Cha, J., Moon, Y.-J., et al. 2021, ApJ, 920, 101
SunPy Community, Barnes, W. T., Bobra, M. G., et al. 2020, ApJ, 890, 68
van der Walt, S., Colbert, S. C., & Varoquaux, G. 2011, CSE, 13, 22
Wang, Y.-M., Biersteker, J. B., Sheeley, N. R., et al. 2007, ApJ, 660, 882
Yashiro, S., Gopalswamy, N., Michalek, G., et al. 2004, JGRA, 109, A07105